RSC Advances

ROYAL SOCIETY OF CHEMISTRY

www.rsc.org/advances

The Chemical Stability of Phosphonium-Based Ionic Liquids under Gamma Irradiation

Ryan P. Morco, Jiju M. Joseph, J. Clara Wren*

Department of Chemistry, University of Western Ontario,

London, Ontario, Canada N6A 5B7

(jcwren@uwo.ca)

Abstract

The effects of γ-radiation on the physicochemical and ion transport properties of phosphonium-based ionic liquids (ILs) were investigated. Five ILs that have different physical properties of hydrophobicity, viscosity and conductivity were studied. Gaseous radiolysis products were analyzed using GC-MS, and the IL phase was analyzed using UV-Vis, FTIR and Raman spectroscopy, and conductivity measurement. The results show that the ILs are relatively resistant to radiolytic degradation, but measurable quantities of small organic species are formed. These arise from the radiolytic dissociation of the P – C bond in the cation moiety. These small organic molecules induce agglomeration within the IL and this results in substantial changes to some of the IL properties.

Keywords:

Phosphonium ionic liquid, gamma-radiolysis, chemical stability, conductivity, spectroscopy

1.0 Introduction

Room temperature ionic liquids (ILs) are organic salts that remain liquid at temperatures below 100°C. Ionic liquids have diverse physicochemical properties that make them candidates for use in many industrial applications including separation technologies.[1] Many ILs are known to be stable in high energy environments and they can be tailored to possess unique solvation properties for coordination and extraction of metal ions from aqueous solutions.[2] The stability of ionic liquids and their extraction capabilities thus make them attractive alternatives to organic solvents used in separation processes that are based on liquid-liquid extraction. One such application is the recovery of uranium and plutonium from used nuclear fuel in spent fuel processing and also in radioactive waste treatment. Ionic liquids selected for this type of application must possess a variety of characteristics in order to carry out an efficient and economic separation process. These properties include: (1) a high intrinsic specificity for complexing with trans-uranic actinides over lanthanides and other fission products (the mix of isotopes contained in spent nuclear fuel), (2) a synthetic route with a high yield, (3) thermal, radiation and chemical stability, (4) an efficient switching mechanism for binding and releasing target elements (in terms of complexation and decomplexation), and (5) a high immiscibility with aqueous solutions. Currently a mixture of 70% kerosene or n-dodecane and 30% tributyl phosphate (TBP) is used in the PUREX process (Plutonium-Uranium Reduction EXtraction) for nuclear fuel reprocessing.[3] In this process the U^{VI} dissolved in a nitric acid solution is extracted as a $UO_2(NO_3)$•2TBP adduct. The solvent in this process is relatively stable with respect to radiation damage, but not the extractant TBP.[3bcdef] The TBP when irradiated undergoes significant dealkylation which greatly affects its extraction specificity over radioactive lanthanides.[3b] However, dealkylation of TBP is not the most important problem with the PUREX

process. One long-standing limitation is the tendency for TBP to form a third phase under high solvent loading conditions.[3f] The TBP complexes form separate, immiscible structured nanophases that create a separate phase. For potential application of the ILs to fuel reprocessing the IL would be the extractant as well as the solvent. Prior to use in nuclear applications where high ionizing radiation fields are present, the radiation stability of candidate ionic liquid extractants must be understood. The effect of radiation on the solvent properties of ILs and how production of radiolysis products may affect the physical properties of the IL as a solvent has to be considered.

Ionic liquids when exposed to radiation may undergo radiolytic decomposition that can alter their physical and chemical properties. Radiolytic decomposition products may also be chemically reactive species which can affect interfacial charge transfer reactions. There are currently only a few published studies on the radiation stability of ILs. Most of this work has used pulse radiolysis and has been confined to ammonium and imidazolium-based ILs. These studies have reported a relatively high radiation resistance for ILs compared to normal organic solvents. This resistance is due to a relatively low probability of 'dry' electrons escaping geminate recombination reactions before they are solvated in an IL.[4] Gamma-radiation stability studies of some ILs are also available, but they too are confined to imidazolium-based ILs.[5] Phosphonium-based ILs, in general, have shown better thermal and redox stabilities than ammonium and imidazolium-based ILs,[6] but have not been as well studied. Most of the radiolysis studies available in literature focus on the initial stages of radiation damage by pulse radiolysis.[3b,7] Steady-state radiolysis studies are also available, but these studies have been limited to the measurement of H_2 production.[3de,7] We have previously reported on the study of steady-state radiolysis of the IL tetradecyl(trihexyl)phosphonium bis(trifluoromethylsulfonyl)

imide (or [P_{14666}] [NTf_2]) alone and in a two phase system with water.[4a] Micelles naturally form in this system due to charge transfer across the phase interface. This effect was accelerated by exposure to γ-radiation due to the generation of small quantities of IL radiolytic decomposition products.[4a]

In this paper, we describe studies on the effects of γ-radiation on the physicochemical and ion transport properties of several phosphonium-based ILs. Five phosphonium-based ILs that have different physical properties, such as hydrophobicity, viscosity, and conductivity (Table 1), were studied. Three of these ILs are hydrophobic, with a long alkyl chain cation (tetradecyl(trihexyl)phosphonium or [P_{14666}]) paired with a different anion: bromide [Br], bis(trifluoromethylsulfonyl) imide [NTf_2], or dicyanamide [DCA], Fig. 1. The two other ILs are water soluble and contain a cation with a shorter alkyl chain (tributylmethylphosphonium or [P_{4441}]) or a short, branched alkyl chain (triisobutylmethylphosphonium or [PTiBMe]). These cations are paired with polyoxygenated ions, methyl sulfate [$MeSO_4$] and tosylate [TsO] respectively (Fig. 1).

Table 1. The physical properties of the ionic liquids investigated (T = 25 °C).

Ionic Liquid	$[P_{14666}]$ [Br]	$[P_{14666}]$ $[NTf_2]$	$[P_{14666}]$ [DCA]	$[P_{4441}]$ $[MeSO_4]$	[PTiBMe] [TsO]
Density (g/ml)[8]	0.9546	1.0652	0.8985	1.0662	1.07
Viscosity (cP)[8]	2094	292.5	280.4	409.3	1320*
Conductivity (μS/cm)	9	108	216	862	92
Miscible with Water[8]	No	No	No	Yes	Yes
Melting Point (°C)[8]	-61	-72	-67	-81.4**	Liquid at RT***
Solubility of H_2O (wt.%)[9]	6.720	0.225	3.407	highly soluble	highly soluble

*: Value reported at 20 ^{o}C.
**: Melting point not observed, value reported is a glass transition temperature.
***: Observed liquid at room temperature

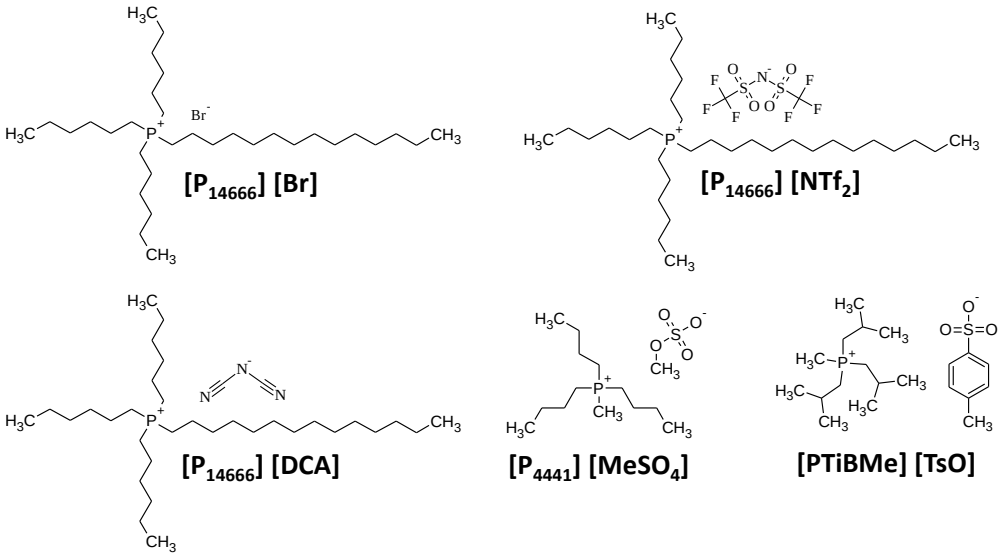

Fig. 1 Structures of the phosphonium-based ionic liquids used in this study.

2.0 Experimental

2.1 Sample Preparation and Irradiation

All five of the ILs used in this study were purchased from Sigma-Aldrich, were of the highest purity available (> 95%) and were used as-received. Samples for irradiation were prepared by placing 2 ml of IL inside a 10-ml pyrex vial (Agilent Technologies). The test vials were prepared inside an argon (Praxair, 99.99% purity) purged glove box to create a deaerated IL system and were sealed with aluminum crimp caps with PTFE/silicone septa. Multiple vials were prepared for tests with different irradiation times. Karl Fischer titration of the ILs after Ar-purging showed that the water contents in the ILs were < 2000 ppm.

Irradiation was carried out in a ^{60}Co gamma cell (MDS Nordion) which provided the irradiation chamber with uniform absorption dose rate of 4.0 kGy·h^{-1} (in water) within the vial

volume. The samples were irradiated for 96 and 192 h providing a total dose of 384 and 768 kGy, respectively. For comparison, the approximate dose equivalent to a one year continuous processing of uranium-based fuels in a commercial facility is 1200 kGy.[5c]

2.2 Analytical Methods

Ionic liquid and headspace gas samples were extracted from the test vials after completion of an irradiation period (normally as soon as reasonably possible). Gas samples were extracted from the vial's headspace using a gas-tight syringe with a Luer lock valve (Agilent Technologies) and were injected into the gas sampling port of a gas chromatograph. The gas chromatograph system consisted of a GS-GASPRO column (0.32-mm I.D. and 60-m long) connected to quadrupole mass selective and thermal conductivity detectors. Volatile organic molecules and hydrogen gas in the headspace were analyzed using helium or nitrogen, respectively, as the carrier gas at flow rate of 4.6 $ml \cdot min^{-1}$.

UV-visible spectrophotometry, Fourier transform infra-red spectroscopy (FTIR), and Raman spectroscopy were used to identify and crudely quantify the species generated by radiolytic decomposition of the target ILs. The UV-Visible spectrophotometry was performed using a diode array spectrophotometer (BioLogic Science Instruments Modular Optical System 450 and ALX 250 lamp with J&M TIDAS NMC 301 detector). The FTIR spectra were collected in the frequency range of 4000 – 600 cm^{-1} using a Bruker Vertex 70v FTIR spectrometer. The FTIR analysis was carried using an attenuated total reflectance (ATR) accessory, with an IL sample placed drop-wise on top of the ATR crystal. Raman spectroscopy analysis was performed using a Renishaw model 2000 Raman spectrometer with a laser excitation wavelength

of 633 nm. The IL samples were analyzed using a set up with the laser focused perpendicularly onto the side of the test vial.

Hydrogen (^{1}H), ^{13}C, ^{31}P and ^{19}F NMR spectroscopy using a Varian INOVA 400 MHz or INOVA 600 MHz spectrometer was performed on both un-irradiated and 192-h irradiated IL samples in deuterated acetone. Chemical shifts were recorded with respect to the reference ^{1}H and ^{13}C peaks of the acetone (2.03 ppm and 28.90 ppm, respectively). The chemical shifts observed for the un-irradiated ILs are listed in Appendix.

Conductivities of the ILs were measured using an electrochemical impedance method with a Solartron potentiostat model 1287 and 1250 Solartron frequency response analyzer that applies a sinusoidal potential wave and measures the cell impedance as a function of frequency over the frequency range of 0.1 Hz to 65 kHz. The conductivity cell consisted of a quartz cuvette with two parallel electrodes made of glassy carbon. The cell constant, the ratio of the gap to the area of the electrodes, was experimentally determined to be 8.6 cm^{-1} using standard solutions of KCl (for which the theoretical conductivity is known). The impedance of the ionic liquid arises from resistive and capacitive contributions and can be described by the following equation,

$$Z = Z_{real} + jZ_{im} = R + j\frac{1}{\omega C} \quad (1)$$

where Z is the impedance, Z_{real} and Z_{im} are the real and imaginary impedance, j is the imaginary unit, R is the resistance, ω is the frequency of the AC potential, and C is the capacitance. The impedance data were plotted in a Nyquist Plot (imaginary vs. real impedance), and the real

impedance value was used to obtain the conductivity. The electrical conductivity, or specific conductance, can be calculated from the following equation,

$$\sigma = \frac{1}{R} \cdot \frac{\ell}{A} \qquad (2)$$

where σ is the specific conductance, R is the resistance, and $\frac{\ell}{A}$ is the cell constant (ℓ is the distance between electrodes and A is the area of the electrodes). Conductivities of the ILs were measured three times and a relative standard deviation of less than 2% was observed for all measurements.

3.0 Results and Discussion

3.1 Airborne Radiolysis Products

The airborne radiolysis products observed in the headspace after irradiation for different time periods for the five ILs are listed in Table 2. In addition to the products listed in the table, there were a few other minor peaks in the GC-MS spectra that were not identified. The concentrations of the organic species observed in the headspace in our study are not quantified in absolute terms because it was difficult to obtain the requisite standard gas samples. However, the concentrations of the airborne species generally increased with irradiation time. The airborne radiolysis products do not constitute a complete set of radiolysis products as non-volatile species would not transfer to the headspace. The airborne decomposition products are organic molecules having a carbon chain length less than C-8. The absence of longer carbon-chain compounds in the headspace may be due to either their low radiolytic yield or their low volatility. Interestingly

we did not observe any C-1 or C-2 compounds, except for CHF_3 and C_2F_6 from the anion of $[P_{14666}]$ $[NTf_2]$.

Table 2. The major radiolytic decomposition products of ionic liquids detected in the gas phase.

Ionic Liquid	Irradiation Time	
	92 h	192 h
$[P_{14666}]$ [Br]	H_2 hexane (C_6H_{14})	H_2 hexane (C_6H_{14}) hexene (C_6H_{12}) propane (C_3H_8)
$[P_{14666}]$ $[NTf_2]$	H_2 hexane (C_6H_{14}) fluoroform (CHF_3) propane (C_3H_8)	H_2 hexane (C_6H_{14}) fluoroform (CHF_3) hexafluoroethane (C_2F_6)
$[P_{14666}]$ [DCA]	H_2 hexane (C_6H_{14})	H_2 hexane (C_6H_{14}) hexene (C_6H_{12})
$[P_{4441}]$ $[MeSO_4]$	H_2 butane (C_4H_{10}) pentane (C_5H_{12}) propane (C_3H_8)	H_2 butane (C_4H_{10}) pentane (C_5H_{12}) propane (C_3H_8) octane (C_8H_{18})
[PTiBMe] [TsO]	H_2 isobutane (C_4H_{10}) isobutylene (C_4H_8) propane (C_3H_8) propene (C_3H_6)	H_2 isobutane (C_4H_{10}) isobutylene (C_4H_8) toluene ($C_6H_5CH_3$) propane (C_3H_8) propene (C_3H_6)

During radiolysis, organic molecules are susceptible to homolytic radical cleavage to form two free radical species.[10] These radical species then react with each other to form stable molecular products. It is therefore expected to see smaller fragments of the IL as a result of the

various bond dissociations that have occurred. Reaction of radical species with the bulk IL through radical addition or H abstraction is also possible. However, we think that the former is less probable since the ILs under consideration here do not have multiple bonds locations that favour radical addition. We also did not detect the formation of double bonds in ILs after irradiation (spectroscopic results presented later). This is consistent with the reported behaviour of this class of IL.[11]

The common airborne products from the ILs containing the cation moiety [P_{14666}] are C-6 carbons, hexane and hexene, whereas those from [P_{4441}] and [PTiBMe] are shorter C-4 or C-5 compounds. These observations are consistent with expectations arising from the bond strengths and the stabilities of the free radicals produced by the radiolytic dissociation of the ILs. In the cation moiety [P_{14666}] the P – C bond is weaker than the C – C bond, and the cation dissociation product is an organic carbon radical. The organic radical stability increases in the order: methyl < primary < secondary < tertiary.[12] Thus, the radiolytic decomposition of [P_{14666}] mainly leads to the formation of a hexyl radical, $\bullet C_6H_{13}$, which then either abstracts or donates $\bullet H$ to a neighbouring IL molecule and forms stable hexane (C_6H_{14}) or hexene (C_6H_{12}) and H_2. Also as expected, we did not detect C-14 compounds in the headspace since these long chained compounds are not volatile and will likely stay in the IL phase. A general degradation scheme for the [P_{14666}] cation based on the gaseous radiolysis products detected is proposed in Scheme 1a.

(a) [P_{14666}] cation

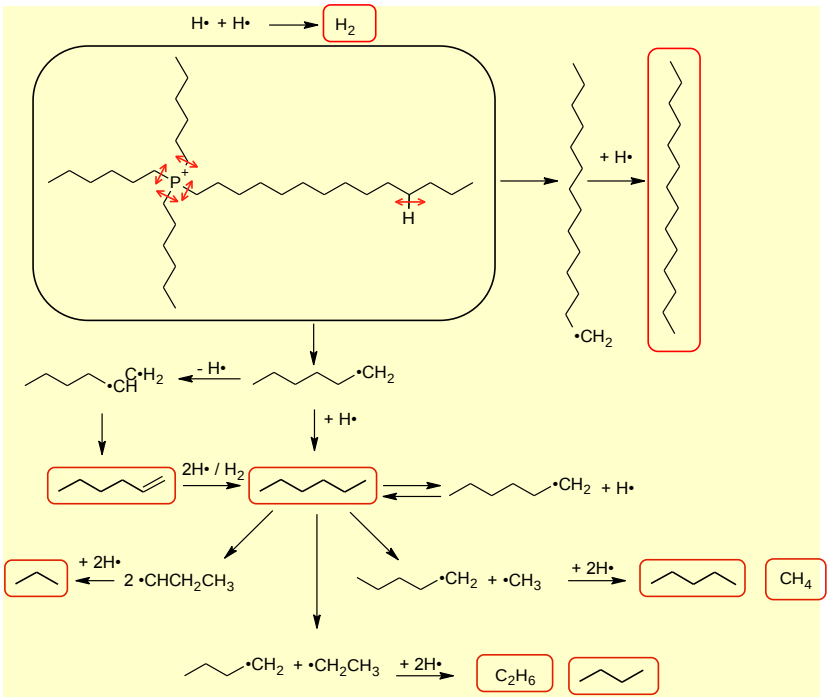

(b) [NTf_2] anion

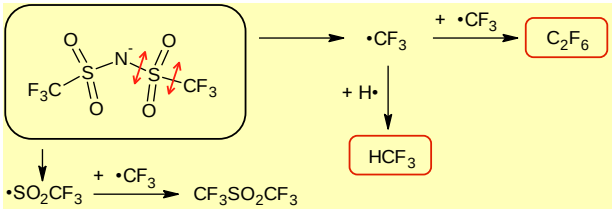

Scheme 1 Proposed degradation scheme pathway of (a) [P_{14666}] cation and (b) [NTf_2] anion during gamma radiolysis.

Similarly, the dissociation of the weaker P – C bond in [P_{4441}] and [PTiBMe] mainly leads to the formation of butyl and isobutyl radicals (•C_4H_9), respectively. For [P_{4441}] which contains normal alkyl chains, the butyl radical undergoes •H abstraction to form butane, abstracts a methyl radical to form pentane (C_5H_{12}), or dimerizes to form octane (C_8H_{18}). However, no significant formation of butene was observed since the formation of a C = C double

bond is less favourable for short alkyl chains. For [PTiBMe], the isobutyl radicals form isobutylene (C_4H_8) as well as isobutane (C_4H_{10}). The [P_{4441}] and [PTiBMe] moieties have a C-1 branch attached to the phosphonium ion. However, the methyl radical ($\bullet CH_3$) arising from P – CH_3 bond cleavage is likely to react with a butyl radical to form pentane as suggested in Scheme 2b. We did not observe any C-1 and C-2 compounds, confirming that the methyl radicals are being consumed up and that the C – C bond cleavage within alkyl chain is less likely than the P – C bond cleavage.

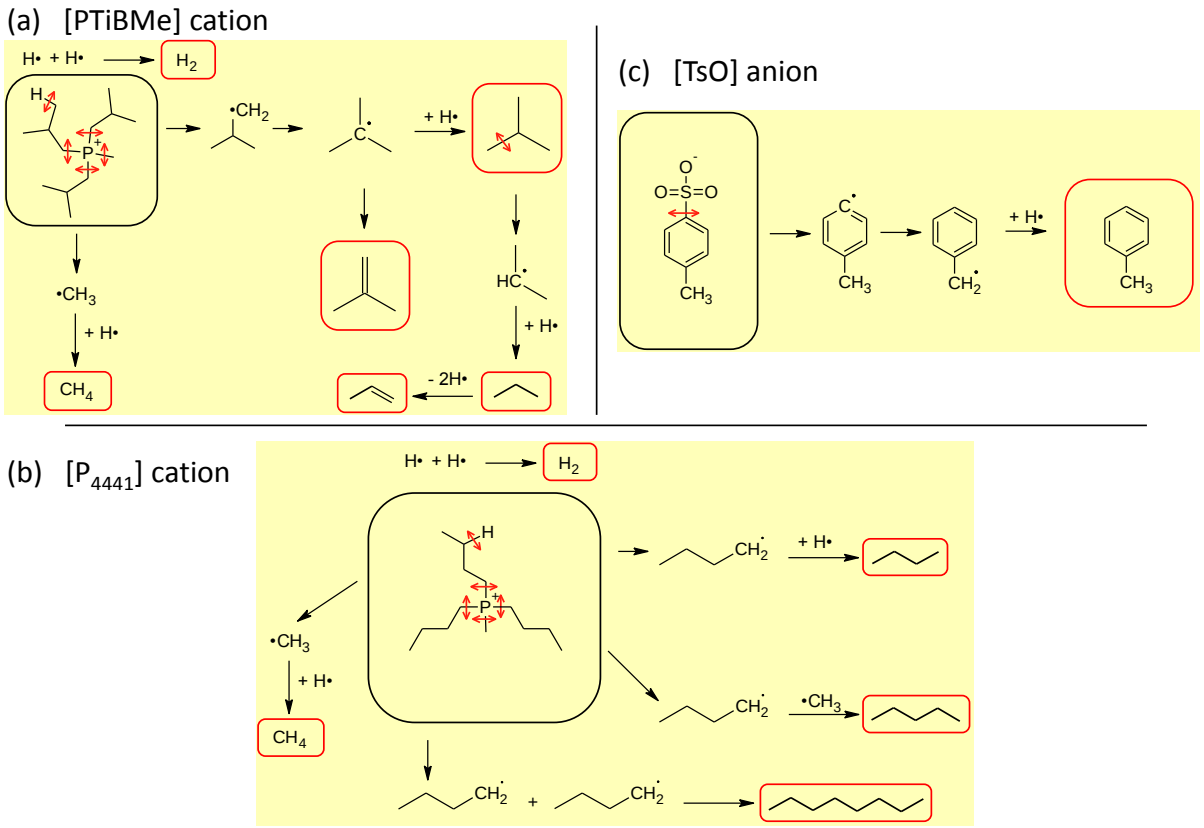

Scheme 1 Proposed degradation scheme pathway of (a) [PTiBMe] and (b) [P_{4441}] cations, and (c) [TsO] anion during gamma radiolysis.

In all of the ILs studied a higher concentration of propane was observed with a longer irradiation time. This indicates that the organic fragments from radiolysis continue to undergo further radiolytic decomposition. Although the production rate of propane in the IL phase may be lower than the production rates of C-4 or C-6 species, propane has a higher vapour pressure and hence becomes airborne[13] more easily. This may result in an apparent higher concentration for propane if we did not achieved full equilibrium between the gas and liquid phases in our vials for the heavier species.

Gamma-irradiation also induces dissociation of the polyatomic anions: the trifluoromethyl radical ($\bullet CF_3$) is formed from [NTf_2] and the benzyl radical ($\bullet C_6H_4CH_3$) is formed from [TsO], as indicated in Schemes 1b and 2c, respectively. These radicals then further react to form CHF_3 and C_2F_6, and toluene ($C_6H_5CH_3$), respectively. No airborne products from the anions were observed following irradiation of the ILs containing [Br], [DCA] and [$MeSO_4$]. Again these observations are consistent with the stabilities of the potential radical products of those anions. The stability of a free radical decreases when the hybridization of the carbon goes from sp^3 to sp^2 to sp.[12b] Thus, it is harder to induce cleavage of the C – N bond of [DCA] to form $\bullet C \equiv N$, and no airborne products associated with this radical were observed. On the other hand, the cleavage of the C – S bond in [TsO] that leads to the formation of $\bullet C_6H_4CH_3$ is more favourable due to the stabilization of that radical by resonance.[12bc, 14] The radiolysis products, CHF_3 and C_2F_6, from [P_{14666}] [NTf_2] were also observed by Le Rouzo et al. following irradiation of butylmethylimidazolium ILs containing the [NTf_2] anion.[10]

The concentration of H_2 in the headspace above [P_{14666}] [NTf_2] and [P_{14666}] [Br] was measured as a function of irradiation time. Gaseous hydrogen is a typical radiolysis product found in irradiated ILs.[3de, 15] It originated from the recombination of •H (which was produced

from homolytic cleavage of the C – H bond, as shown in the degradation pathway in Schemes 1a and 2ab) and from abstraction of a hydrogen atom from the neighbouring IL molecule by •H radical.[3de] The concentration of H_2 was converted to the total number of mols of H_2 in the headspace per IL mass (mol/kg), and plotted as a function of accumulated dose in kGy in Fig. 2. The production of H_2 in the headspace increases linearly with irradiation time or accumulated dose. The net radiation chemical yields for H_2 production (g-value) determined from the slopes in Fig. 2 are 0.05 and 0.04 μmol·J^{-1} for [P_{14666}] [NTf_2] and [P_{14666}] [Br], respectively. These g-values are about five times lower than the g-value (0.25 μmol·J^{-1}) reported for a similar IL but with longer alkyl substituted chains [P_{14888}] [NTf_2]. [3e] The difference in the g-values may be attributed to the different ILs but also to the different dose rates and radiation sources used in the two studies. The rate of H_2 production in the headspace depends on IL-gas interfacial mass transfer as well as the radiolytic production of H_2 in the IL phase, and will depend on the dose rate (3 Gy·s^{-1} in reference [3e] versus 1.11 Gy·s^{-1} in this study). Nevertheless it should be noted that the g-values for H_2 production from the ILs are lower than the g-value for H_2 production from *n*-hexane (0.55 μmol·J^{-1}).[16] The g-value for H_2 production provides a limit on the radiolytic decomposition; if all of the H_2 is generated from •H formed from an initial C – H bond dissociation, a g-value of 0.05 μmol·J^{-1} corresponds to approximately 0.06% C – H bond dissociation in the ILs. The hydrogen yield can also be used to estimate the concentration of the other radiolysis products. For example the ratio of the peak areas of hexene to hexane in the gas chromatogram was 1:45. The H_2 yields obtained in our study are ~0.05 μmol•J^{-1}. The g-value for hexane is expected to be much smaller. Assuming that the g-value of hexane is as high as the g-value for H_2, the g-value for hexene would be about 0.001 μmol•J^{-1}.

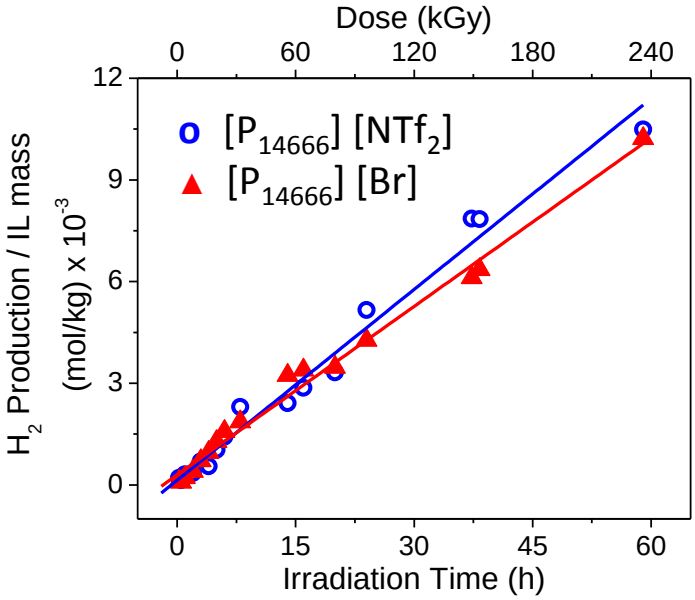

Fig. 2 Production of H_2 as a function of irradiation time.

3.2 NMR Analysis

There was no observed difference between the ^{1}H, ^{13}C, and ^{31}P NMR spectra of non-irradiated and irradiated ILs for all the samples except for $[P_{4441}]\,[MeSO_4]$. The irradiated $[P_{4441}]\,[MeSO_4]$ showed the following additional peaks: ^{1}H NMR: δ 8.27 (s), 4.60 (s), 4.56 (s); ^{13}C NMR: δ 110.2, 41.37, 37.85, 34.10, 33.38, 32.98, 32.54; and ^{31}P NMR: δ 41.37, 37.85, 34.10, 33.38, 32.98, 32.54, 30.37. The ^{19}F NMR spectrum for irradiated $[P_{14666}]\,[NTf_2]$ also displayed an additional peak at -80.73 ppm. These may indicate the presence of newly formed radiolytic products from $[P_{4441}]\,[MeSO_4]$ and $[P_{14666}]\,[NTf_2]$. However, the intensities of the new NMR peaks in these ILs were extremely low, and it was not possible to assign the observed peaks to any molecular structures. The inability to see differences between the NMR spectra of irradiated and unirradiated samples is normally considered to correspond to less than 1%

impurity in the substance being analyzed. These results are consistent with the qualitative findings of low concentrations of degradation products by GC-MS as well as the low g-value for H_2 production.

3.3 Spectroscopic Analyses of the IL Phases

The changes in the IL phase due to γ-radiation were examined using UV-Vis, FTIR and Raman spectroscopic tools and the analysis results are presented in Figs. 3 to 7. In discussing the spectroscopic results, the ILs are considered in two groups: (1) the ILs containing the $[P_{14666}]$ cation and different anions, and (2) the ILs containing cations with shorter alkyl chains, $[P_{4441}]$ $[MeSO_4]$ and [PTiBMe] [TsO].

3.3.1 The $[P_{14666}]$ ILs

The colour of $[P_{14666}]$ [Br] changed from pale yellow to a darker yellow with increasing irradiation time (Fig. 3). The corresponding UV-Vis, FTIR and Raman spectra of the IL are also shown in Fig. 3. The UV-Vis spectrum of the un-irradiated $[P_{14666}]$ [Br] has a main peak near 290 nm with two minor peaks near 350 nm and 475 nm. Since this IL does not have a polyatomic anion, it is safe to assign these absorption bands to electronic transitions of the IL cation moiety; the anion can affect the transition probabilities. The main absorption band at 290 nm shows an increase in absorption intensity with irradiation time, but no significant broadening of the band or red shift of the peak was observed. When the peak intensity was normalized with respect to the peak height, the absorption band at 290 nm has the same profile for irradiated and un-irradiated samples. This absorption band is also observed for $[P_{14666}]$ $[NTf_2]$ (see Fig. 4 later). We have not been able to assign this band to any specific electronic transition, but suspect that the probability of this transition is increased by irradiation due to a change in the cation

configuration around radiolytically-formed small organic molecules, see further discussion in Section 3.3.2.

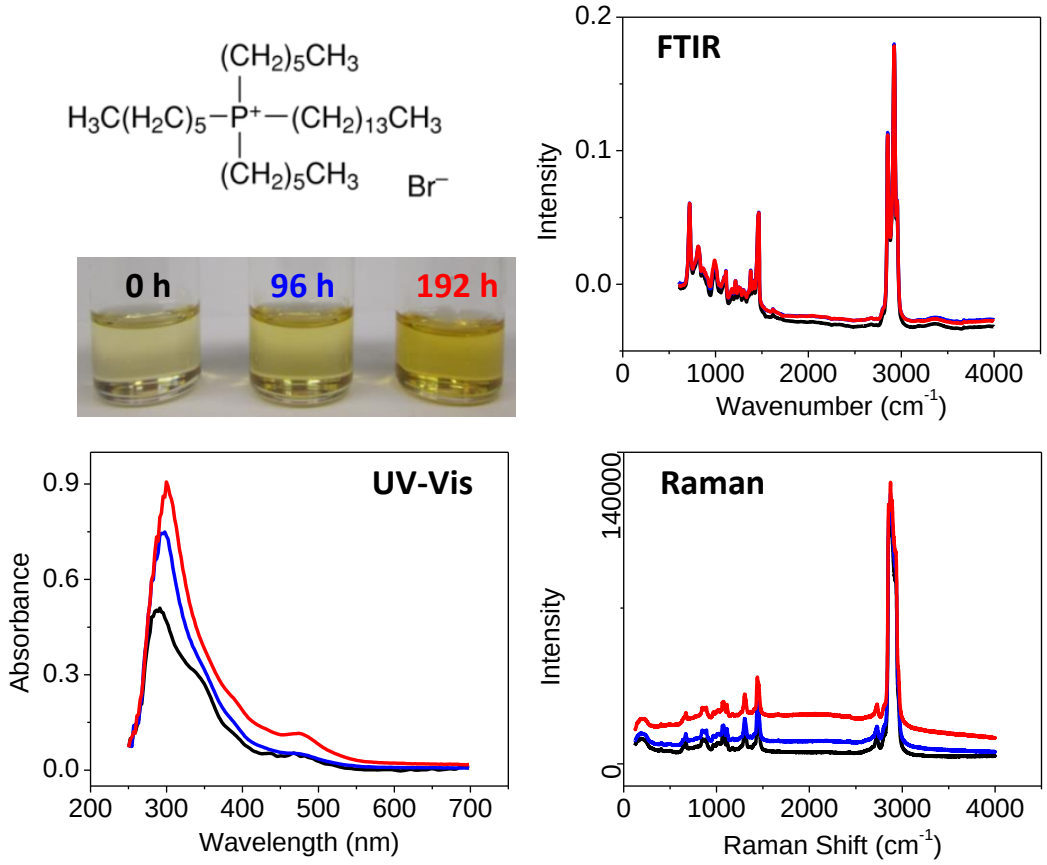

Fig. 3 Photographs of irradiated [P_{14666}] [Br] and the corresponding UV-Vis, FTIR and Raman spectra as a function of irradiation time. Black, blue and red lines are for 0, 96 and 192 h of irradiation, respectively.

The corresponding FTIR and Raman spectra did not show any new peaks or relative changes in their intensities after irradiation, except for a small increase in the broad band intensity in the Raman spectrum. This broad band was present and its intensity increased with irradiation in the Raman spectra of the all three [P_{14666}] ILs studied, albeit with different

intensities, see below. The absence of any new peaks in the IR region is evidence that the quantities of radiolysis products in the ILs are relatively low.

The $[P_{14666}]$ $[NTf_2]$ IL is colourless prior to irradiation but slowly becomes yellow with irradiation (Fig. 4). The UV-Vis spectrum of the un-irradiated IL has only a single, small absorption band near 290 nm, the same location as a band observed for $[P_{14666}]$ [Br] (Fig. 3). The presence of only one UV-absorption band at a wavelength longer than 250 nm is consistent with the DFT calculation for this IL reported in literature.[17] That calculation predicts that there

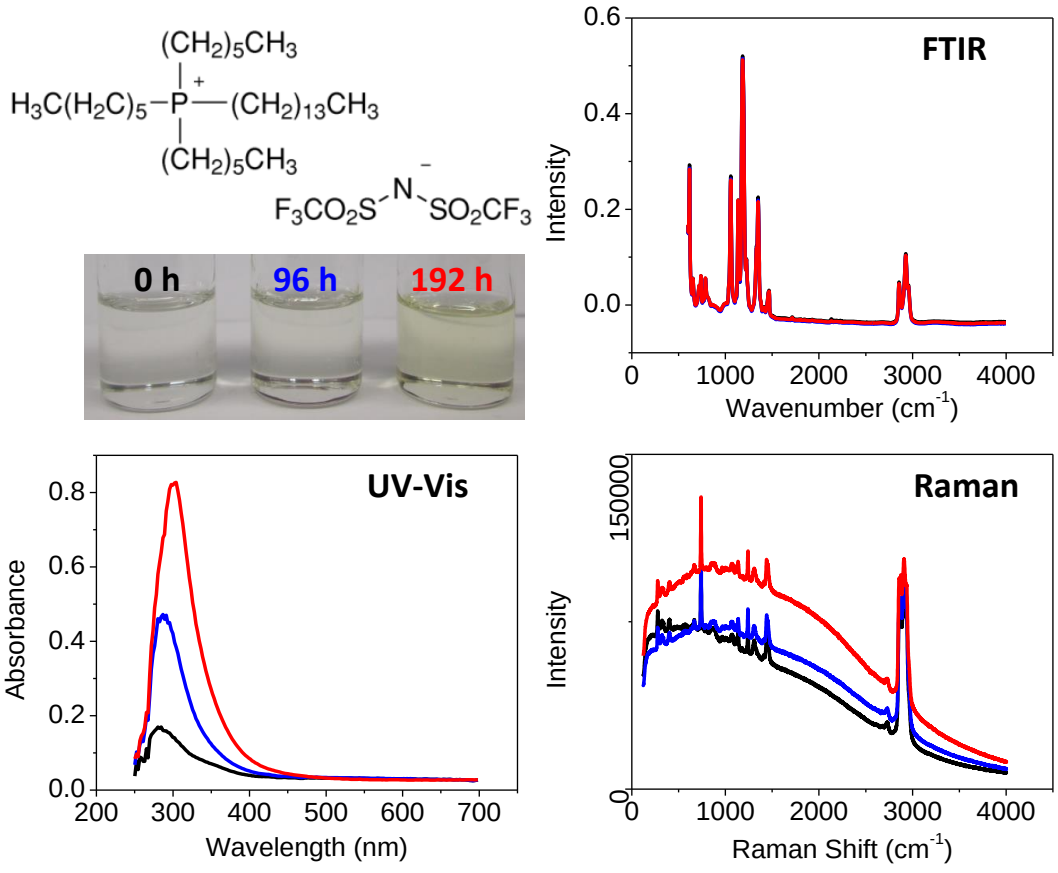

Fig. 4 Photographs of irradiated $[P_{14666}]$ $[NTf_2]$ and the corresponding UV-Vis, FTIR and Raman spectra as a function of irradiation time. Black, blue and red lines are for 0, 96 and 192 h of irradiation, respectively.

are a smaller number of allowed electronic transitions in this wavelength range for $[P_{14666}]$ $[NTf_2]$ compared to $[P_{14666}]$ [Br].[17] As observed for $[P_{14666}]$ [Br], the intensity of the 290 nm absorption band increased with irradiation time. Although we see the radiolytic decomposition products, CHF_3 and C_2F_6, from the anion moiety $[NTf_2]$ in the headspace, these molecules do not absorb light at wavelengths > 250 nm and hence we did not see any UV absorption corresponding to these species. No changes in the rotational-vibrational transition peaks in the corresponding FTIR and Raman spectra were observed for either IL as a function of irradiation time. The main difference observed between the two ILs is that the scattering background is higher in the Raman spectrum of $[P_{14666}]$ $[NTf_2]$ compared to the spectrum of $[P_{14666}]$ [Br].

As discussed in more detail later, the increase in the intensity of the 290 nm band with irradiation time for both $[P_{14666}]$ $[NTf_2]$ and $[P_{14666}]$ [Br] can be attributed to conformational changes in the IL molecules rather than to the formation of new chromophores. It has been established that a conformational change in a molecule can change the probability (or oscillator strength) of an electronic transition without affecting the excitation energy. A review by Tsuji et al.[18] of the theoretical and experimental studies on the conformational effect on tetrasilane electronic transitions has shown that it is not the excitation energy but the intensity of the transitions that changes significantly as the SiSiSiSi dihedral angle varies, and that a similar conformational effect has been found for a series of hexasilane conformers. We believe that the required conformational changes are likely in the IL system, based on our experience with the irradiation of $[P_{14666}]$ $[NTf_2]$)/water systems and the enhanced formation of micelles caused by irradiation. [4a]

The [P_{14666}] [DCA] IL shows the most colour change when irradiated, going from pale yellow, to yellow, and then to dark orange (Fig. 5). The main UV-Vis absorption band for this IL has a peak at ~305 nm, a slightly longer wavelength than the main absorption bands observed for [P_{14666}] [Br] and [P_{14666}] [NTf_2]. This shift was predicted by DFT calculations reported elsewhere.[17]

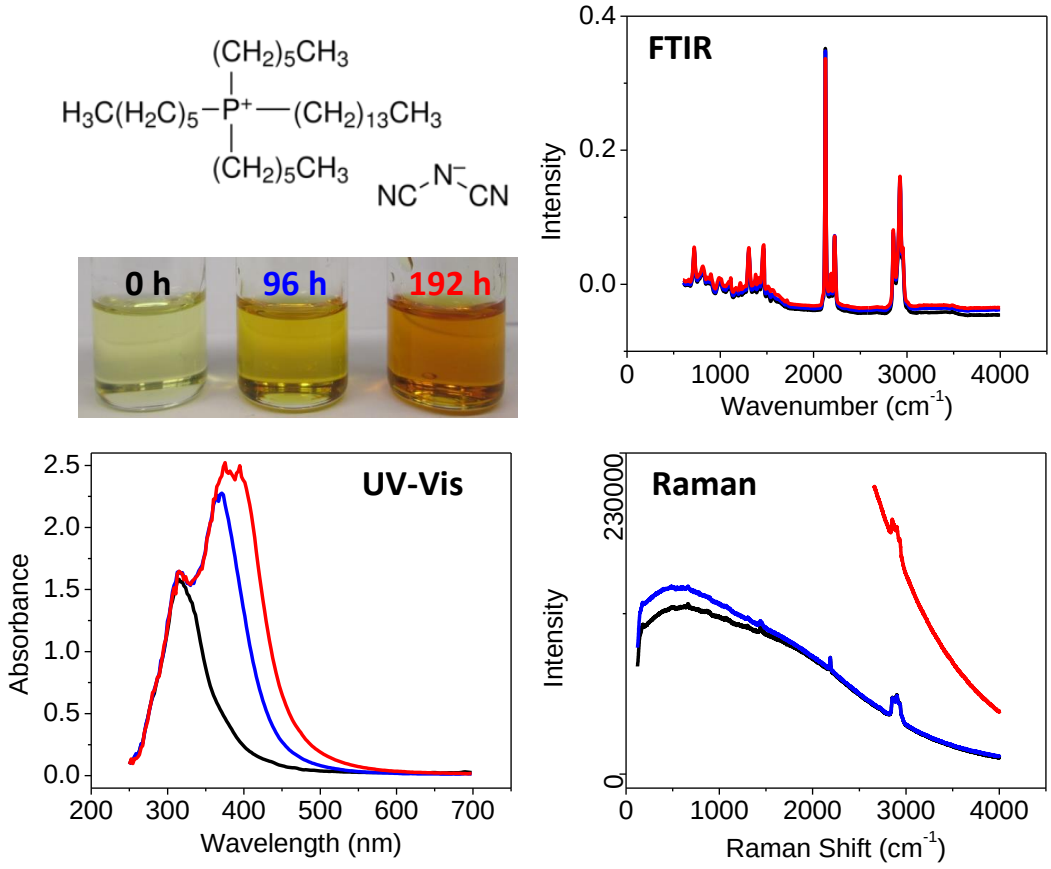

Fig. 5 Photographs of irradiated [P_{14666}] [DCA] and the corresponding UV-Vis, FTIR and Raman spectra as a function of irradiation time. Black, blue and red lines are for 0, 96 and 192 h of irradiation, respectively.

The UV-Vis spectra of [P_{14666}] [DCA] also had an additional absorption band near 370 nm whose intensity is very small for the un-irradiated IL. While the intensity of the 305 nm

band does not change significantly, the intensity of the 370 nm band increases dramatically after 96 h and 192 h of irradiation. The increase in absorption of blue light accounts for the yellow appearance of the irradiated IL. (Note that the absorbance at 370 nm for the sample irradiated for 192 h is greater than 2.5, the detection limit of the instrument.) The 370 nm band is assigned to an electronic energy transition within the [DCA] anion moiety. The oscillator strength of this transition is very small when the [DCA] anion is not confined. However, the study by Zhang et al.[19] on the effect of confinement in nano-scale matrices on the emission and fluorescence spectra of dicyanamide anion-based ILs has shown that the intensity of the emission band is nearly 3 orders of magnitude higher when the IL is confined in mesoporous silica gel. In our system, we do not have such a confinement, but we can have a conformational change in the IL molecule caused by rearrangement around small organic radiolysis products.

As for the other ILs, no additional peaks or changes in the relative intensities of the sharp, well-defined FTIR peaks were observed after irradiation. However, the Raman scattering intensity of the broad band increased greatly with irradiation of [P_{14666}] [DCA] compared to the other two ILs.

3.3.2 Summary on the [P_{14666}] ILs

All three of the [P_{14666}] ILs studied had the same airborne radiolytic decomposition products from the cation moiety [P_{14666}]. In all three ILs, there are no observable changes in the FTIR spectra, no new peaks in the Raman spectra, and no significant red shifts in the UV-Vis absorption spectra. However, the intensities of the UV-Vis bands at 290 nm, for [P_{14666}] [Br] and [P_{14666}] [NTf_2], and at 370 nm for [P_{14666}] [DCA], increased with increasing irradiation time. Accompanying these change are changes in the Raman scattering intensities of the broad bands.

These results are consistent with only small radiolytic decomposition yields for the [P_{14666}] ILs, and an indirect impact on the spectra caused by the decomposition products.

A change in molecular conformation of the ILs does not change the electronic excitation energy and shift band positions, but it can influence the electronic transition probabilities and hence the intensities of the UV-Vis absorption bands. The studies on radiolysis of ILs using short-term (ns to ps scale) radiation pulses have reported that the presence of water at an impurity level can have a considerable effect on the UV-Vis absorbance observed immediately following radiation pulse.[20] However, there is some uncertainty regarding the species that are responsible for the absorbance in the 500-1500 nm range, ranging from solvated electron to the F-centres created in the quasi-ordered IL structure and electronically excited IL molecule, and the effect of water present at an impurity level on the absorbance. Irrespective of the assignments of these peaks, their absorbance decrease very rapidly in less than 1 μs. This is evidence that transient radiolysis products such as excited species, F-centres and solvated electron are responsible for this absorption. Our UV-Vis spectra also show negligible absorbance in the 500-1500 nm range, further confirming the transient nature of the absorbance Our results show that stable radiolytic decomposition products may be present in the ILs but they do not have large extinction coefficient in the 500-1500 nm range.

The increase in the Raman scattering intensity of the broad band with irradiation is also attributed to a change in molecular conformation of the ILs. It should be noted that the excitation wavelength used in the Raman spectroscopy in this study was 633 nm. The UV-Vis spectra of the un-irradiated and irradiated ILs show negligible absorbance at this wavelength and hence, we ruled out the contribution of fluorescence to the broad Raman bands. On the other hand, the intensity of the broad Raman band increases with irradiation and this increase is much

more pronounced for the ILs with low viscosities, while it has no correlation with the solubility of water in these ILs. Thus, we attribute the increase in the broad band intensity with irradiation to the fact that the radiolytic decomposition products induce a more pronounced change on the conformation by allowing more aggregates to form (see further discussion below).

Comparison of the spectra of the three [P_{14666}] ILs provides an interesting observation. In Raman spectra of the un-irradiated ILs the scattering intensity of the broad band is larger in the order: [P_{14666}] [DCA] > [P_{14666}] [NTf_2] > [P_{14666}] [Br] (negligible), whereas the UV-Vis absorbance is larger in the order: [P_{14666}] [DCA] > [P_{14666}] [Br] > [P_{14666}] [NTf_2]. For the un-irradiated samples, the order of the UV-Vis absorbance near 350 nm (blue) is more closely associated with the order of the intensity of the colour change: P_{14666}] [DCA] (most yellowish) > [P_{14666}] [Br] > [P_{14666}] [NTf_2] (colourless), as expected, because the increased absorbance in the blue regions makes the solutions appear yellow.

The Raman scattering intensity of the broad band increases with irradiation for all three ILs. However, the increase is more pronounced near 2000 cm^{-1} for the [Br] and [NTf_2] ILs, whereas it is more pronounced near 500 cm^{-1} for the [DCA] IL. The increase in the Raman scattering intensity of the broad band is modest after 96 h irradiation and it is more pronounced after 192-h irradiation; the effect is not linear with irradiation dose. On the other hand, the UV-Vis absorbance appears to increase nearly proportionally with irradiation time, and the increases in the intensities of both the UV-Vis and the Raman scattering are in the order:

[P_{14666}] [DCA] > [P_{14666}] [NTf_2] > [P_{14666}] [Br]

This is the same order as the intensities of the Raman broad band of the un-irradiated samples. Comparison of the physical properties of the ILs (Table 1) shows that the order listed

immediately above follows the order for the conductivities and the inverse order for the viscosities of the ILs.

These observations are consistent with increasing numbers of IL molecules experiencing molecular conformational changes (that are caused by aggregation) as small organic radiolysis products accumulate. These organic molecules can act as hydrophobic sites that promote reorientation (and/or aggregation) of the long organic chains of the IL cations and act as centres of micelles.[4a] The formation of an aggregate can strengthen the ionic bond (or the Coulombic attraction) between the cation and anion centres of the IL molecules. Light scattering is enhanced by the increase in the concentration of the aggregates or micelles, increasing the Raman scattering intensity of the broad band. The aggregation of IL molecules occurs more easily in a less viscous IL, hence the IL with the lowest viscosity, $[P_{14666}]$ [DCA], has the biggest Raman change. The radiolytic chemical decomposition yields are too small for the species to be observed as distinct peaks in the FTIR and Raman spectra of irradiated ILs, but the effect of even small numbers of such species is magnified by their ability to affect multiple IL molecules as aggregation nuclei.

3.3.3 Short Carbon Chain ILs

Gamma-irradiation of $[P_{4441}]$ $[MeSO_4]$ leads to no apparent colour change (Fig. 6). The UV-Vis spectra of this IL have a band at 250 nm that increases in intensity after irradiation. However, this IL has no significant absorbance at wavelengths longer than 350 nm and hence it remains colourless, even after irradiation. Like the $[P_{14666}]$ ILs, the FTIR and Raman spectra of this IL also have no additional peaks or changes in the relative intensities of the sharp and distinct peaks with irradiation. Unlike the $[P_{14666}]$ ILs where irradiation increases the Raman

scattering intensity of the broad band, the initial broad peak at ~ 1700 cm^{-1} for $[P_{4441}]$ $[MeSO_4]$ disappeared after 96 h of irradiation. This peak is attributed to the presence of water in the IL.[4a, 21] This IL is miscible with water and hygroscopic ILs are known to absorb water from the air, so the presence of dissolved water as an impurity is very likely. We are not sure why the 'water band' disappeared after irradiation. It may have been due to radiolytic decomposition of the

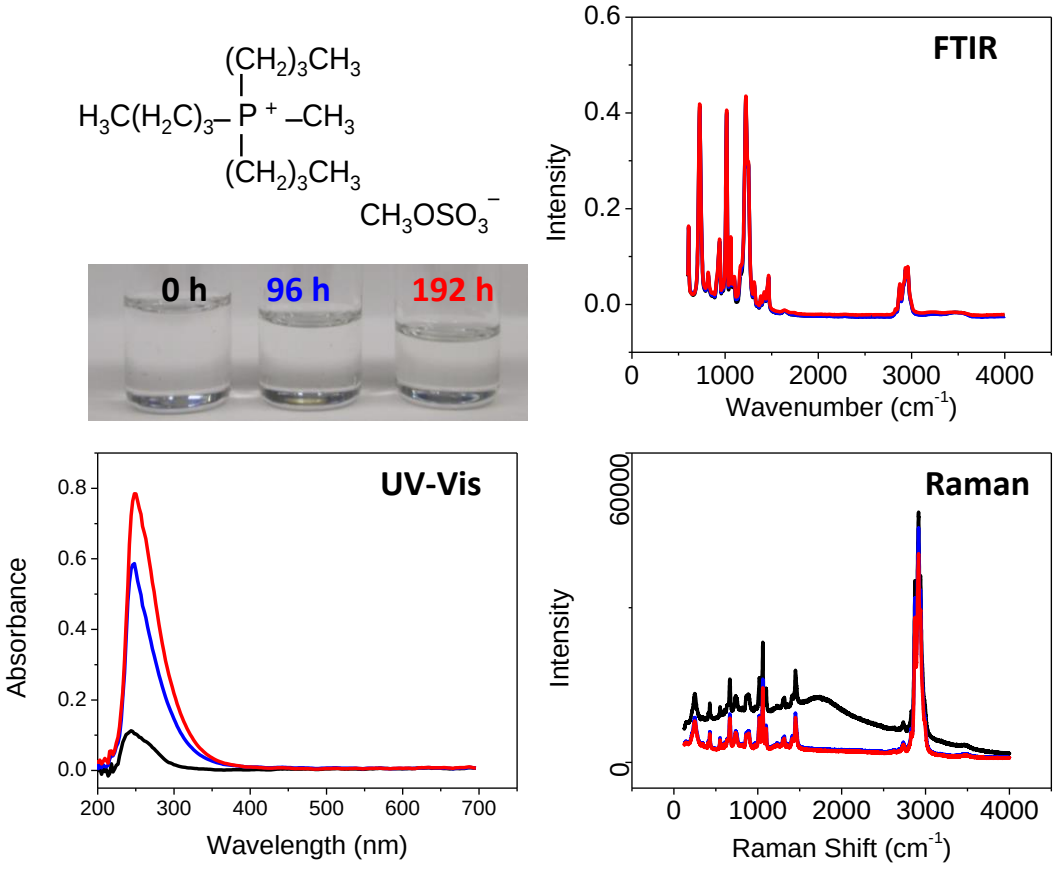

Fig. 6 Photographs of irradiated $[P_{4441}]$ $[MeSO_4]$ and the corresponding UV-Vis, FTIR and Raman spectra as a function of irradiation time. Black, blue and red lines are for 0, 96 and 192 h of irradiation, respectively. The blue and red lines are heavily overlapping in the Raman and FTIR spectra.

water and reaction of water radicals with the IL, or reaction of water molecules with organic radicals, as levels too low to create measurable quantities of reaction products. We did not see any water in the headspace gas during GC-MS analysis.

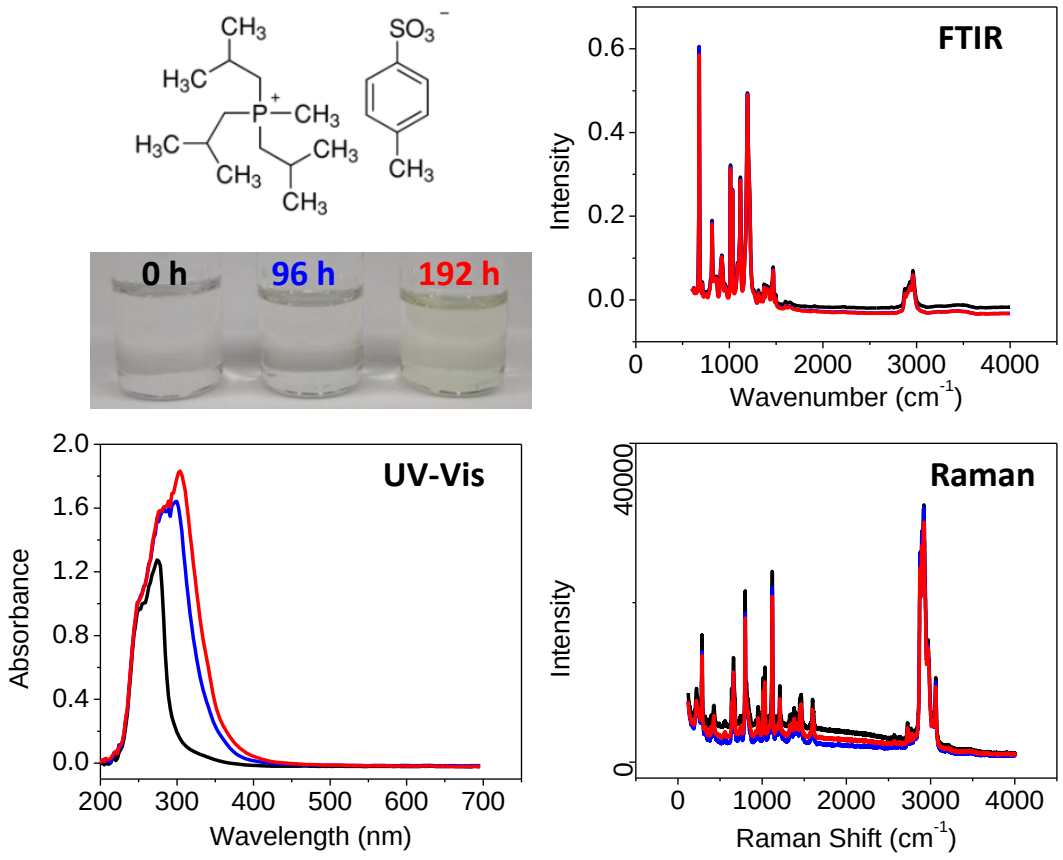

Fig. 7 Photographs of irradiated [PTiBMe] [TsO] and the corresponding UV-Vis, FTIR and Raman spectra as a function of irradiation time. Black, blue and red lines are for 0, 96 and 192 h of irradiation, respectively.

The un-irradiated [PTiBMe] [TsO] is colourless; it changes to pale yellow with exposure to radiation (Fig. 7). The UV-Vis absorption spectrum of the un-irradiated IL has peaks at 250 nm and 275 nm. The first peak matches the 250 nm peak seen for [P_{4441}] IL and the peaks of both of these ILs are shorter in wavelength than the peaks observed for the [P_{14666}] ILs. The

shorter wavelengths for the peaks of the [P_{4441}] and [PTiBMe] ILs are consistent with the expectation of larger HOMO-LUMO energy gaps for the shorter carbon chained compounds.[18,22] The UV-Vis absorption spectra of the irradiated [PTiBMe] IL show increases in the bands at 250 nm and 275 nm with increased irradiation and the appearance of an additional peak at around 300 nm. The latter accounts for the colour change with irradiation. Like all of the other ILs, the FTIR and Raman spectra of this IL show no significant difference with irradiation time. As observed for [P_{4441}] [$MeSO_4$], there is a broad Raman scattering band that disappeared with irradiation. As for the [P_{4441}] IL this IL is also miscible with water and a microemulsion of water impurities could have produced the scattering background.

3.3.4 Summary on the Short Carbon Chain ILs

As observed for the [P_{14666}] ILs, the short carbon chain ILs, [P_{4441}] [$MeSO_4$] and [PTiBMe] [TsO], have airborne radiolytic decomposition products from the cation moieties but only [PTiBMe] [TsO] has decomposition products from the anion moiety (Table 2). In both short carbon chain ILs, there are no observable changes in the FTIR and the Raman spectra. There are significant red shifts in the UV-Vis absorption spectra and the UV-Vis absorbances, near 250 nm for [P_{4441}] [$MeSO_4$] and near 275 nm and 300 nm for [PTiBMe] [TsO], increase with irradiation time. However, unlike the [P_{14666}] ILs, there are no changes in the Raman scattering intensity of the broad band with irradiation time.

Again, the increases in the UV-Vis absorbance with irradiation time observed for the short carbon chain ILs are attributed to conformational changes of the IL molecules due to orientation of the organic tails around small organic molecules produced by radiolytic decomposition. However, the orientation of these IL molecules is not likely to be as highly

structured, nor will those ILs form large aggregates or micelles as easily as the longer chain containing [P_{14666}] ILs.

3.4 Conductivity

The changes in the conductivities of the ILs as a function of irradiation time are shown in Fig. 8. The conductivity of an IL with an initially low conductivity, such as [P_{14666}] [Br] and [PTiBMe] [TsO], does not change significantly with increasing irradiation time. However, the conductivity of an IL with an initially higher conductivity decreases with irradiation time; the rate of decrease slows down with time, eventually reaching a steady state value. After 192 h irradiation, the conductivity of the water soluble [P_{4441}] [$MeSO_4$] IL decreased by about 50% (from 862 to 446 $\mu S \cdot cm^{-1}$) whereas the conductivity of the hydrophobic [P_{14666}] [DCA] IL decreased by only about 25% (from 216 to 161 $\mu S \cdot cm^{-1}$).

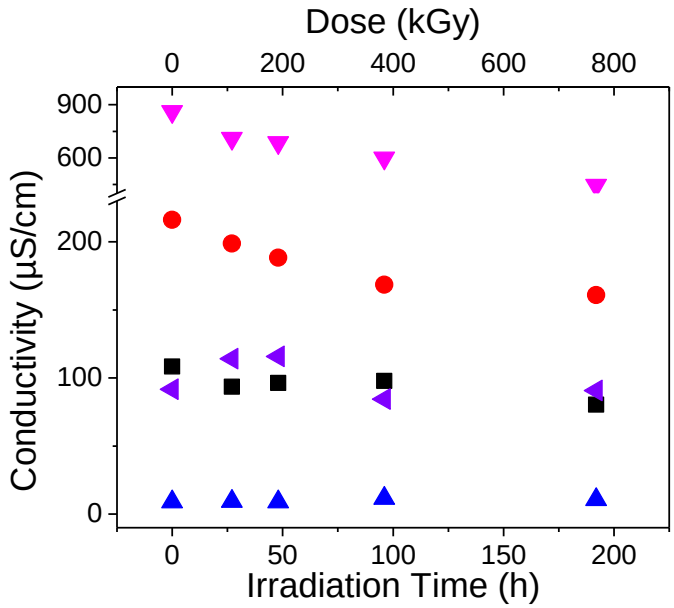

Fig. 8 Conductivities of phosphonium ILs as a function of irradiation time: ● [P_{14666}] [DCA], ▲ [P_{14666}] [Br], ■ [P_{14666}] [NTf_2], ◀ [PTiBMe] [TsO] and ▼ [P_{4441}] [$MeSO_4$].

The conductivity of an electrolyte is known to be inversely proportional to the viscosity of the medium according to the Walden's law.[23] The conductivity of an IL, in a particular highly viscous IL, is known to deviate from the Walden's law due to significant ion pairing and the addition of small organic molecules to a highly viscous IL is known to increase its conductivity.[23,24] This, however, is not the case in this study. As the concentration of small organic compounds increases in an IL, more IL molecules reorient themselves around these organic molecules. The IL cations and anions rearrange themselves such that their ion pairing is strengthened, as noted earlier. Such conformational changes in the IL reduce the mobility of the cations and anions of the IL molecules. This has the effect of lowering the conductivity of the IL, as we have seen. The observed changes in conductivity with irradiation are consistent with the changes observed in the UV-Vis absorbances.

3.5 Comparison with Other Studies on the Irradiation of ILs

Previous studies on the effect of γ-radiation on imidazolium-based ILs have also reported an increase in their UV-Vis absorbance due to irradiation.[5, 25] In these studies the increase in absorbance was attributed to the formation of radiolysis products that have stronger light absorption than the original IL molecule. In this study on phosphonium-based ILs, we observed the production of organic compounds with carbon lengths ranging from C-3 to C-8. The absence of smaller organic compounds in the gas phase indicates that for the cation moiety, P – C bond dissociation is the preferred radiolytic decomposition pathway over C – C bond dissociation. The organic radicals formed after bond dissociation can readily react with •H via free radical addition or can extract •H from neighbouring IL hydrocarbons to form non-radical species. These short chain hydrocarbons do not absorb light at wavelengths > 250 nm and are more likely to absorb light at even shorter wavelengths than the larger original IL. The organic radicals

could theoretically initiate a chain reaction leading to polymerization of the organic chains. If this occurred to any great extent we would expect to see broadening of the peaks in the FTIR and Raman spectra, but we did not observed any such broadening of the rotational-vibrational peaks. The low concentrations of organic species that were detected in the gas phase and the negligible changes in the NMR, FTIR and Raman spectra indicate that the net radiolytic chemical decomposition yield of the ILs studied here is very low, even after 192 h irradiation at 4.0 kGy·h^{-1} (for a total radiation dose of 768 kGy).

In this study we see changes in the UV-Vis spectra despite a low level of radiolytic decomposition. However, the changes involve increases in the absorption intensity of one or two bands without accompanying changes in the band positions. For the ILs with long alkyl chains these changes in UV-Vis spectra accompany changes in the broad band Raman scattering intensity. We believe that the increase in UV absorbance is due to conformational change brought by reorientation of the IL molecules around the radiolytically-produced small organic compounds. The change in molecular conformation can influence the electronic transition probability in the UV-Vis spectrum, the light scattering probability in the Raman spectrum, and the conductivity of the IL solutions. As noted above, our results show that any stable radiolytic decomposition products, if present, do not have large extinction coefficients in the 500-1500 nm range and hence, their fluorescence cannot account for the broad Raman bands. In the wavelength range shorter than 500 nm, the UV-Vis absorption spectra show larger increases in intensity at the longer wavelengths, indicating that these changes are not due to UV-Vis absorption by small IL decomposition products.

It has also been reported that γ-radiation of an IL induces a colour change even when there is negligible radiolytic chemical decomposition.[5,25] These studies have attributed those

colour changes to the creation of F-centers or the formation of a new species.[3c,5d,24] F-centers are crystallographic defects in which an anionic vacancy in a crystal is filled by one or more electrons.[3c,26] The electrons can occupy electronic energy states in which they can absorb visible light. F-centers occur in salt crystals, particularly metallic oxides, when heated or irradiated.[27] Solvated or hydrated electrons in a liquid phase also show a similar light absorption capability; the hydrated electron absorbs light at around 720 nm and this light absorption property is extensively employed in the study of radiation-induced chemistry in water or organic solvents.[27] Studies on water and organic species radiolysis have also shown that the lifetime of solvated electrons in liquid phases is very short due to their high chemical reactivity (a lifetime of less than 1 ms in neutral water at 25 ^{o}C).[4c] It is possible that radiolysis of an IL liberates an electron that could be 'solvated' by the IL to behave like a quasi F-center. Although the lifetime of a 'solvated' electron in more viscous ILs might be expected to be much longer than the typical lifetime of a solvated electron in water, it is difficult to imagine that quasi F-centers or 'solvated' electrons could survive for extremely long times in an irradiated IL. In our experiments the colour change induced by irradiation did not fade, even during long-term storage (weeks) at room temperature after the irradiation period had ended. Hence we do not believe that quasi F-centers exist in our ILs.

The effects of water and air on IL radiolysis have been previously studied in imidazolium[25b], ammonium[28] and phosphonium[4a] types of ILs. Results show that water and air do not alter the radiolytic yields in the [BuMeIm] [NTf_2] and [N_{4441}] [NTf_2] ILs with water concentrations ranging from 360 ppm to 15558 ppm.[25b,28] Also, γ–irradiated phosphonium ILs in contact with water showed negligible radiolytic degradation[4a]. However the water promotes an

accelerated phase mixing process. We believe that the effect of water on the irradiation of the ILs done in this study was also negligible.

4.0 Conclusions

The effects of γ-radiation on the physicochemical and ion transport properties of phosphonium-based ILs were investigated. Five ILs that have different hydrophobicities, viscosities and conductivities were studied. Radiolysis product analysis was performed by measuring products that migrated to the gas phase using GC-MS. The IL phase was analyzed using UV-Vis, NMR, FTIR and Raman spectroscopy, and conductivity measurement.

Extended gamma irradiation (at doses up to ~ 1 MGy) does not induce substantial chemical decomposition of the IL molecules into smaller fragments. However, the small amounts of organic species that are formed can induce conformational changes as the IL molecules reorient themselves around the small organic molecules. Although the change in molecular conformation does not affect the electronic energy levels in the ILs, it can influence the electronic transition probability and hence the intensity of an UV-Vis absorption band. In the ILs with long alkyl chains, the reorientation of the IL molecules around the small organic products can form larger aggregates or micelles which can increase light scattering probability, and decrease the conductivity of the IL.

5.0 Acknowledgements

Financial support for this work was provided by an NSERC (Natural Science and Engineering Research Council of Canada) Discovery grant. Support from the Canada Foundation for Innovation New Opportunity grant and the Ontario Research Fund Excellence in

Research: Nuclear Ontario grant is greatly acknowledged for the purchase of the UV-Vis absorption and FTIR spectrometers, respectively. The authors would also like to thank Drs. Susan Howett and James Wishart for their helpful inputs on the short-term pulse radiolysis data.

6.0 References

1. (a) A. Heintz, *J. Chem. Thermodyn*., 2005, **37**, 525,; (b) R.D. Rogers and K.R. Seddon, eds., *Ionic Liquids as Green Solvents: Progress and Prospects*, ACS, Washington, DC, 2003; (c) J. F. Wishart, Energy Environ. Sci., 2009, **2**, 956; (d) H. Zhao, S. Q. Xia and P.S. Ma, *J. Chem. Technol. Biotechnol*., 2005, **80**, 1089.

2. S. Dai, Y.H. Ju and C.E. Barnes, *J. Chem. Soc. Dalton Trans*., 1999, **24**, 1201.

3. (a) S.H. Ha, R.N. Menchavez and Y.M. Koo, *Korean J. Chem. Eng*., 2010, **27**, 1360; (b) I.A. Shkrob, S.D. Chemerisov and J.F. Wishart, *J. Phys. Chem*. B, 2007, **111**, 11786; (c) J.F. Wishart and I.A. Shkrob, *The Radiation Chemistry of Ionic Liquids and its Implications for their Use in Nuclear Fuel Processing*, in *Ionic Liquids: From Knowledge to Application*, American Chemical Society, 2009, **1030**, 119; (d) S.B. Dhiman, G.S. Goff, W. Runde and J.A. LaVerne, *J. Nucl. Mater*., 2014, **453**, 182; (e) P. Tarabek, S.Y. Liu, K. Haygarth, and D.M. Bartels, *Radiat. Phys. Chem*., 2009, **78**, 168; (f) P.R.Vasudeva Rao and Z.Kolarik, *Solvent Extr. Ion Exch*., 1996, **14**, 955.

4. (a) S.E. Howett, J.M. Joseph, J.J. Noël and J.C. Wren, *J. Colloid Interface Sci*., 2011, **361**, 338; (b) J. Grodkowski, P. Neta and J.F. Wishart, *J. Phys. Chem*. A, 2003, **107**, 9794; (c) J.F. Wishart, *Radiation Chemistry of Ionic Liquids: Reactivity of Primary Species*, in *Ionic Liquids as Green Solvents: Progress and Prospects*, eds. R.D. Rogers and K.R. Seddon, ACS, Washington, DC, 2003.

5. (a) M.Y. Qi, G.Z. Wu, Q.M. Li and Y.S. Luo, *Radiat. Phys. Chem*., 2008, **77**, 877; (b) C. Jagadeeswara Rao, K.A. Venkatesan, B.V.R. Tata, K. Nagarajan, T.G. Srinivasan and P.R. Vasudeva Rao, *Radiat. Phys. Chem*., 2011, **80**, 643; (c) N.J. Bridges, A.E. Visser, M.J. Williamson, J.I. Mickalonis and T.M. Adams, *Radiochim. Acta*, 2010, **98**, 243; (d) M.Y. Qi, G.Z. Wu, S.M. Chen and Y.D. Liu, *Radiat. Res*., 2007, **167**, 508; (e) L.Y. Yuan, J. Peng, L. Xu, M.L. Zhai, J.Q. Li and G.S. Wei, *Radiat. Phys. Chem*., 2009, **78**, 1133; (f) L.Y. Yuan, J. Peng, M.L. Zhai, J.Q. Li and G.S. Wei, *Radiat. Phys. Chem.*, 2009, **78**, 737.

6. (a) K.J. Fraser and D.R. MacFarlane, *Aust. J. Chem*., 2009, **62**, 309; (b) J. Luo, O. Conrad and F.J. Vankelecom, *J. Mater. Chem*., 2012, **22**, 20574; (c) A.M. O'Mahony, D.S. Silvester, L. Aldous, C. Hardacre and R.G. Compton, *J. Chem. Eng. Data*, 2008, **53**, 2884.

7. B.J. Mincher and J.F. Wishart, *Solvent Extr. Ion Exc*., 2014, **32**, 563.

8. (a) Cytec product sheet CYPHOS®, https://www.cytec.com/specialty-chemicals/ionicliquidstable.htm <Accessed: February 26, 2013>; (b) S.P.M. Ventura, J. Pauly, J.L. Daridon, J.A. Lopes da Silva, I. M. Marrucho, A.M.A. Dias and J.A.P. Coutinho, *J. Chem. Thermodyn*., 2008, **40**, 1187; (c) A.B. Pereiro, H.I.M. Veiga, J.M.S.S. Esperança and A. Rodríguez, *J. Chem. Thermodyn*., 2009, **41**, 1419.

9. M.G. Freire, P.J. Carvalho, R.L. Gardas, L.M.N.B.F. Santos, I.M. Marrucho and J.A.P. Coutinho, *J. Chem. Eng. Data*, 2008, **53**, 2378.

10. G. Le Rouzo, C. Lamouroux, V. Dauvois, A. Dannoux, S. Legand, D. Durand, P. Moisy and G. Moutiers, *Dalton Trans*., 2009, **31**, 6175.

11. (a) B. Taylor, P.J. Cormier, J.M. Lauzon and K. Ghandi, *Physica B*, 2009, **404**, 936; (b) J.M. Lauzon, D.J. Arseneau, J.C. Brodovitch, J.A.C. Clyburne, P. Cormier, B. McCollum and K. Ghandi, *Phys. Chem. Chem. Phys*., 2008, **10**, 5957; (c) K. Ghandi, *Green Sustainable Chem*., 2014, **4**, 44.

12. (a) A.A. Zavitsas, D.W. Rogers and N. Matsunaga, *J. Org. Chem*., 2010, **75**, 5697; (b) D.C. Nonhebel and J.C. Walton, *Free-radical Chemistry; Structure and Mechanism*, Syndics of the Cambridge University Press, London, UK, 1974; (c) J. Clayden, N. Greeves, S. Warren and P. Wothers, *Organic Chemistry*, Oxford University Press Inc., New York, USA, 2001.

13. H.S. Myers, *Ind. Eng. Chem*., 1955, **47**, 1659.

14. A.A. Zavitsas, *J. Org. Chem*., 2008, **73**, 9022.

15. (a) S.B. Dhiman, G.S. Goff, W. Runde, J.A. LaVerne, *J. Phys. Chem. B*, 2013, **117**, 6782; (b) Dhiman, S. B.; LaVerne, J. A., *J. Nucl. Mater*., 2013, **436**, 8.

16. (a) T.J. Hardwick, *J. Phys. Chem*., 1960, **64**, 1623; (b) A.A. Garibov, K.T. Eyubov, T.N. Agaev, *High Energ. Chem*., 2004, **38**, 295.

17. R.P. Morco, A.Y. Musa and J.C. Wren, *Solid State Ionics*, 2014, **258**, 74.

18. H. Tsuji, J. Michl and K. Tamao, *J. Organomet. Chem*., 2003, **685**, 9.

19. J. Zhang, Q. Zhang, F. Shi, S. Zhang, B. Qiao, L. Liu, Y. Ma and Y. Deng, *Chem. Phys. Lett*., 2008, **461**, 229.

20. (a) J.F. Wishart, P. Neta, *J. Phys. Chem. B*, 2003, **107,** 7261; (b) S.E. Howett, *Investigating the Effects of Radiation on Phosphonium-Based Ionic Liquids*, University of Western Ontario - Electronic Thesis and Dissertation Repository Paper 1639, 2013. http://ir.lib.uwo.ca/etd/1639

21. (a) G.E. Walrafen and L.A. Blatz, *J. Chem. Phys*., 1973, **59**, 2646; (b) D.M. Carey and G.M. Korenowski, *J. Chem. Phys*., 1998, **108**, 2669;

22. Y. Cao, Y. Chen, X. Sun and T. Mu, *Clean-Soil Air Water*, 2014, **42**, 1162.

23. P.C. Trulove and R.A. Mantz, *Electrochemical Properties of Ionic Liquids*, in *Ionic Liquids in Synthesis*, eds. P. Wasserscheid and T. Welton, Wiley-VCH Verlag, Weinhein, Germany, 2008.

24. (a) R.L. Perry, K.M. Jones, W.D. Scott, Q. Liao and C.L. Hussey, *J. Chem. Eng. Data*, 1995, **40**, 615; (b) Q. Liao and C.L. Hussey, *J. Chem. Eng. Data*, 1996, **41**, 1126.

25. (a) D. Allen, G. Baston, A.E. Bradley, T. Gorman, A. Haile, I. Hamblett, J.E. Hatter, M.J.F. Healey, B. Hodgson, R. Lewin, K.V. Lovell, B. Newton, W.R. Pitner, D.W. Rooney, D. Sanders, K.R. Seddon, H.E. Sims and R.C. Thied, *Green Chem*., 2002, **4**, 152; (b) L. Berthon, S. I. Nikitenko, I. Bisel, C. Berthon, M. Faucon, B. Saucerotte, N. Zorz and P. Moisy, *Dalton Trans*., 2006, **21**, 2526.

26. (a) C.J. Delbecq, P. Pringsheim and P. Yuster, *J. Chem. Phys*., 1951, **19**, 574; (b) N. J. Kreidl and J. R. Hensler, *J. Am. Ceram. Soc*., 1955, **38**, 423.

27. (a) G.V. Buxton, C.L. Greenstock, W.P. Helman and A.B. Ross, *J. Phys. Chem. Ref. Data*, 1988, **17**, 513; (b) J.W.T. Spinks and R.J. Woods, *An Introduction to Radiation Chemistry*, Wiley, New York, 1990.

28. E. Bosse, L. Berthon, N. Zorz, J. Monget, C. Berthon, I. Bisel, S. Legand and P. Moisy, *Dalton Trans.*, 2008, **7**, 924.

Appendix: Characteristic NMR Peaks Observed for the Un-Irradiated ILs

[P_{14666}] [Br]. ^{1}H NMR (399.764 MHz, Acetone-*d6*): δ 2.52 (m, 8H), 1.68-1.47 (m, 32H), 1.31-1.25 (m, 16H), 0.87-0.83 (m, 12H). ^{31}P NMR (161.831 MHz, Acetone-*d6*): δ 33.24

[P_{14666}] [DCA]. ^{1}H NMR (399.764 MHz, Acetone-*d6*): δ 2.38 (m, 8H), 1.68-1.47 (m, 32H), 1.31-1.25 (m, 16H), 0.87-0.83 (m, 12H). ^{13}C NMR (150.745 MHz, Acetone-*d6*): δ 31.71, 30.80, 30.56, 30.46, 30.26, 30.17, 22.40, 22.10, 21.10, 21.06, 18.45, 18.13. ^{31}P NMR (161.831 MHz, Acetone-*d6*): δ 33.61.

[P_{14666}] [NTf_2]. ^{1}H NMR (399.764 MHz, Acetone-*d6*): δ 2.38 (m, 8H), 1.68-1.47 (m, 32H), 1.31-1.25 (m, 16H), 0.87-0.83 (m, 12H). ^{13}C NMR (150.745 MHz, Acetone-*d6*): δ 31.71, 30.78, 30.52, 30.42, 30.23, 30.13, 22.40, 22.08, 21.06, 21.03, 18.41, 18.10. ^{31}P NMR (161.831 MHz, Acetone-*d6*): δ 33.64. ^{19}F NMR (563.987 MHz, Acetone-*d6*): δ -79.91.

[PTiBMe] [TsO]. ^{1}H NMR (599.422 MHz, Acetone-*d6*): δ 7.66 (d, 2H), 7.08 (d, 2H), 2.44 (dd, 6H), 2.29 (s, 3H), 2.21 (m, 3H), 2.14 (d, 3H), 1.11 (d, 18H). ^{13}C NMR (150.741 MHz, Acetone-*d6*): δ 146.91, 137.44, 127.77, 126.05, 29.84, 29.53, 23.89, 23.83, 23.79, 23.29, 23.26, 20.27, 6.47, 6.14. ^{31}P NMR (242.667 MHz, Acetone-*d6*): δ 29.15.

[P_{4441}] [$MeSO_4$]. ^{1}H NMR (599.422 MHz, Acetone-*d6*): δ 3.48 (s, 3H), 2.42 (m, 6H), 1.99 (d, 3H), 1.65 (m, 6H), 1.50 (sex, 6H), 0.95 (t, 9H). ^{13}C NMR (150.741 MHz, Acetone-*d6*): δ 52.26, 23.66, 23.55, 23.08, 12.74, 3.19, 2.84. ^{31}P NMR (242.661 MHz, Acetone-*d6*): δ 37.00, 32.3, 32.21.